공학석사학위논문

New methods for simultaneous measurement of R_2, R_2', R_2^*, QSM, positive and negative susceptibility maps using mGESFIDE acquisition

mGESFIDE 신호 획득을 통해 R_2, R_2', R_2^*,
정량적 자화율 영상, 양과 음의 자화율 영상을
동시에 측정하는 새로운 방법

2018년 8월

서울대학교 대학원
컴퓨터공학부
신 동 명

New methods for simultaneous measurement of R_2, R_2', R_2^*, QSM, positive and negative susceptibility maps using mGESFIDE acquisition

지도교수 신 영 길

이 논문을 공학석사 학위논문으로 제출함
2018년 4월

서울대학교 대학원
컴퓨터공학부
신 동 명

신동명의 공학석사 학위논문을 인준함
2018년 6월

위 원 장 이 종 호 (인)
부 위 원 장 신 영 길 (인)
위 원 오 세 홍 (인)

요약

New methods for simultaneous measurement of R_2, R_2', R_2^*, QSM, positive and negative susceptibility maps using mGESFIDE acquisition

신동명
컴퓨터공학부
공과대학
서울대학교

자기공명영상(Magnetic Resonance Imaging, MRI)은 핵자기공명 원리를 이용한 비침습적 영상법이다. 컴퓨터 단층촬영과 다르게 자기공명영상은 신체에 가해진 라디오파에 따라 공명하는 수소 원자핵에서 나오는 신호를 측정함으로 인체에 무해하다는 특징을 가진다. 또한, 자기공명영상은 영상 촬영 시에 발생시키는 라디오파를 각기 다른 세기와 순서로 발생시킴으로서 인체 조직의 특성을 반영하는 다양한 영상을 만들어 낼 수 있다. 하지만 컴퓨터 단층촬영에 비해 상대적으로 긴 영상 시간이 자기공명영상의 임상적 활용을 제한해 왔다.

본 연구에서는 modified gradient-echo sampling of FID and echo (mGESFIDE) 신호를 이용하여 단 5분의 촬영 시간으로 R_2, R_2', R_2^*, 정량적 자화율 영상, 양의 자화율 영상, 음의 자화율 영상을 모두 획득할 수 있는 새로운 영상처리 방법을 제시한다. 먼저 본 연구에서는 mGESFIDE 신호를 라디오 주파수의 형태와 B_1 자기장의 불균일성을 고려하여 보정한 새로운 R_2와 R_2' 영상 구성 방법을 제시한다. 다음으로 mGESFIDE 신호의 모든 메아리의 위상 값을 사용하여 국소 자기장 변화를 측정하는 새로운 방법도 제시한다.

이러한 방법의 유효성을 검증하기 위해서 인 비보(In vivo)의 뇌 영상을 촬영한 뒤 기존의 방법들과 비교를 한다. 본 연구에서 제안한 새로운 영상처리 방법은 임상적 응용이 가능한 고속 영상법이 될 수 있을 것으로 기대된다.

주요어 : Magnetic Resonance Imaging, GESFIDE, R_2, R_2', R_2^*, Quantitative Susceptibility Mapping
학 번 : 2016-21214

Table of Contents

List of Figures

1. Introduction

1.1 Nuclear Magnetic Resonance

Atoms with an odd number of protons posses a nuclear spin angular momentum and exhibit the nuclear magnetic resonance phenomenon (NMR). This nuclei is often referred to as spins and usually described by the spinning charged sphere. In biological systems, hydrogen (^1H) is most abundant and therefore most sensitive signal sources of MR imaging. The spins are oriented randomly in the absence of an external magnetic field. When the external magnetic field is applied, the individual spins have tendency to orient in the direction of the external field and the non-zero net magnetic moment (M_0) is created **(Fig. 1)**.

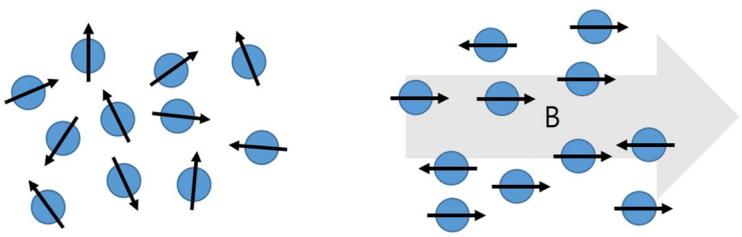

Figure 1. Description of biological system with spins. Black arrows represents rotational axis of each spins. (A) spins are oriented randomly without the external magnetic field. (B) after the external magnetic field is applied, net magnetic moment is created because spin have tendency to align with the external magnetic field.

In the presence of the external magnetic field (B), the nuclear spins exhibit resonance at frequency so called *Larmor frequency* (w).

$$w = \gamma B \qquad \text{[Eq. 1]}$$

γ is called the gyromagnetic ratio which is unique constant for each type of atom and $\gamma/2\pi$=42.57 MHz/Tesla for ^{1}H.

To obtain a signal from the biological spin system, radio frequency (RF) magnetic pulse called B_1 together with the strong static magnetic field (B_0) is applied in the xy plane perpendicular to the B_0 field direction as seen in **Figure 2**. The B_1 field is much weaker (a small fraction of Gauss; 10^4 Gauss = 1 Tesla) than B_0 field (3~11.7 Tesla) and tuned to the resonance frequency of the spins. As a result, the B_1 field tilts the net magnetization moment toward the xy plane according to **Eq. 1** depending on the strength of B_1 and its duration. This phenomenon is called excitation **(Fig. 2)**.

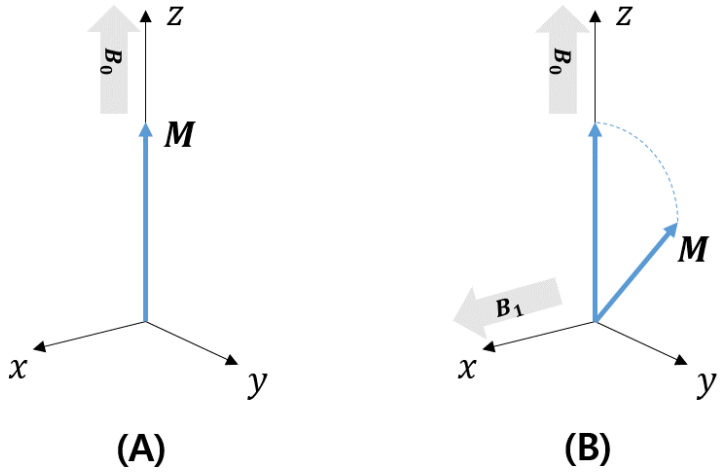

Figure 2. Description of excitation. Here, B_0 field is applied along the z direction while B_1 field is applied along the x direction. (A) before the B_1 field is applied, the non-zero magnetization moment along the z direction is present. (B) B_1 field tuned to resonance frequency of the spins tilts the net magnetization moment (**M**) toward the xy plane. In this figure, $w_0 (=\gamma B_0)$ is demodulated for convenience.

After turning the excitation off, the magnetization vector precess in the xy plane and this precession behaves like small oscillator inducing an electromotive force (EMF) in an nearby coils. Then, these coils generate the signal which is called *free induction decay* (FID). The ensemble of signals measured by many repetitive recording of FID are the basic building blocks of MR imaging. Later, visualization of body is achieved through mapping the spatial information of this tiny oscillator by controlling its relative phases and frequencies

1.2 Bloch Equation

The phenomenon of spin system back to the equilibrium state with an external magnetic field is called *relaxation.* The time constant describing the recovery of the longitudinal (z directional) magnetization vector is called T_1 while the time constant characterizing the decay of transverse magnetization vector is called T_2. Relaxation always occur except when the magnetization vector resides in the equilibrium state **(Fig. 3)**. Therefore, the magnitude of FID is actually decaying until the transverse magnetization fully vanishes **(Fig. 4)**.

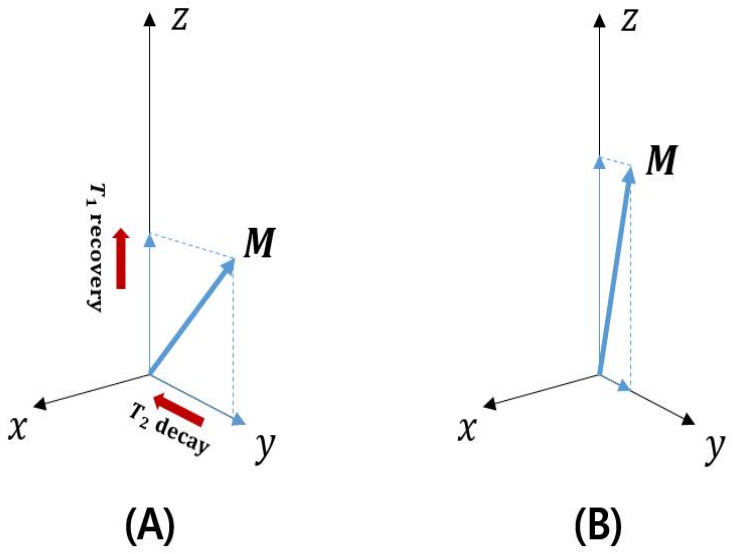

Figure 3. Description of relaxation. (A) The longitudinal magnetization vector recovers to the M_0 while the transverse magnetization vector keeps decaying. (B) after some time later, the magnetization vector has different magnitude of transverse and longitudinal components.

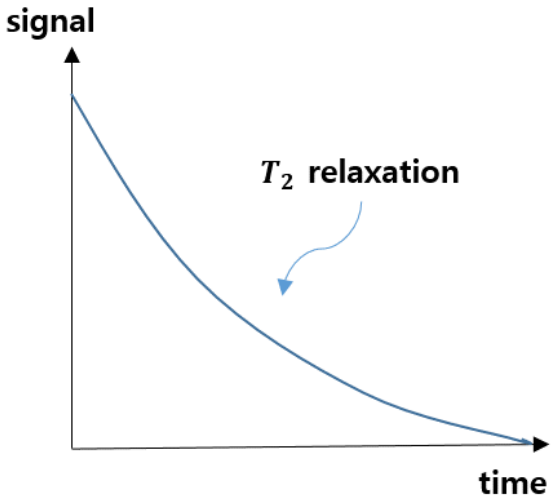

Figure 4. An example of T_2 decaying signal. T_2 relaxation occurs as time progresses until the transverse magnetization fully vanishes. The magnitude of signal decays exponentially. In this figure, $w_0 (=\gamma B_0)$ is demodulated for convenience.

The behavior of the magnetization vector **M** is described by the so called Bloch equation.

$$\frac{d\mathbf{M}}{dt} = \mathbf{M} \times \gamma\mathbf{B} - \frac{M_x\mathbf{i} + M_y\mathbf{j}}{T_2} - \frac{(M_z - M_0)\mathbf{k}}{T_1} \qquad \text{[Eq. 2]}$$

i,**j** and **k** are unit vectors in the x,y and z directions. M_0 is the magnitude of magnetization vector in equilibrium state. **B** comprises all applied magnetic fields including B_0 and B_1.

1.3 Image Formation

Although there are diverse MR imaging methods developed, principle of conventional MR image formation is basically described by a well known mathematical transform: Fourier transform. In 2D MR imaging, linearly increasing magnetic fields called *gradient* (G) in x and y directions are adopted to encode spatial information by weighting the amplitude distribution m(x,y) with an particular frequency after excitation. For example, the spins will have spatially varying phase by applying linear gradient field G_y in y direction when recording the FID **(Fig. 5)**. In this manner, data representing the Fourier decomposition of m(x,y) are acquired by changing the strength and duration of linear gradient fields.

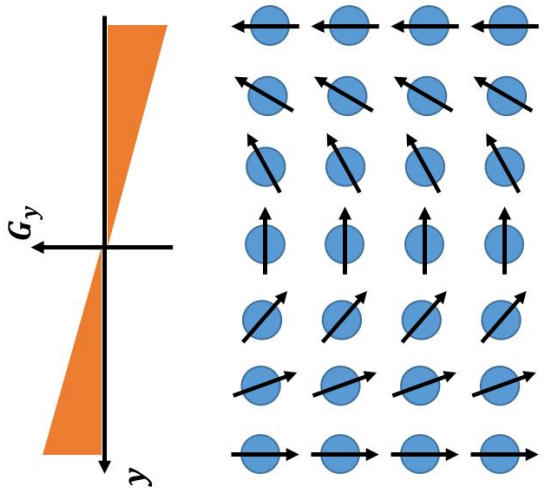

Figure 5. Linear gradient field G_y induces the spins to have different phases according to their positions. This results in weighting the amplitude distribution m(x,y) with an particular frequency so that the Fourier decomposition of m(x,y) is achieved.

This measurements repeat until the sufficient range of data in Fourier domain called *k−space* are filled. Then, a simple 2D Fourier transform is used to reconstruct original distribution m(x,y) **(Fig. 6)**.

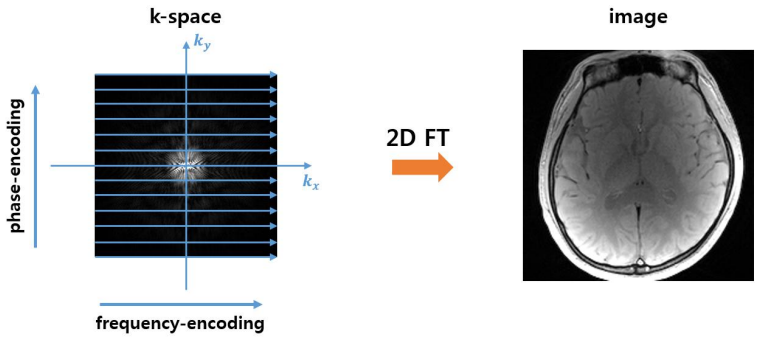

Figure 6. Illustration of k-space and image after fourier transform. Sufficient range of data in k-space need to be measured to reconstruct image. In conventional data acquisition, k-space data is acquired line by line along the *phase-encoding* direction while the one line of k-space data is acquired along the *frequency-encoding* direction.

1.4 Pulse Sequence

Pulse sequence is a set of instructions changing magnetic fields to generate MR signals. Each sequence have a number of parameters such as time to echo (TE), time to repetition (TR) and flip angle (FA). Here, one of the most frequently used pulse sequence called *spin echo* is shown in **Figure 7**. The simplest form of the spin echo consists of 90° and 180° RF pulses and then the acquisition of echo.

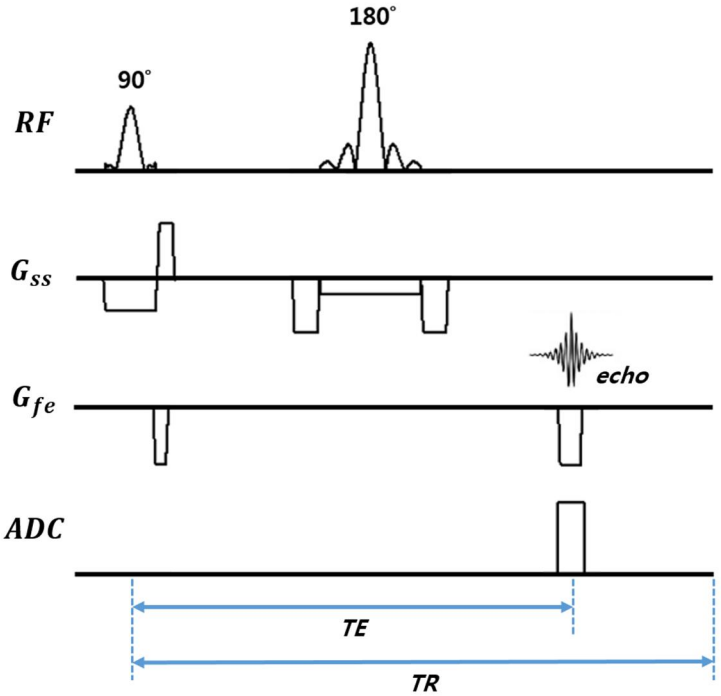

Figure 7. Spin echo pulse sequence diagram. The simplest form of spin echo consists of 90° and 180° RF pulses and then the acquisition of echo. The 180° pulse induces phase reversal of stationary spins whose phases have been scattered by the field inhomogeneities.

Flip angle means how much the magnetization vector would be nutated after RF pulse. Time to echo is the time between the center of an excitation pulse and measured echo. Time to repetition is the time from the application of an excitation pulse to the next one. By changing these parameters, one can acquired the desired image contrasts such as T_1 weighted, T_2 weighted and proton density (PD) weighted images [1] **(Fig. 8)**. It was discovered that tumor tissues have significantly different T_1 and T_2 values compared to the

normal ones [2]. Until now, various type of pulse sequences were developed to reveal the composition and characteristics of tissues.

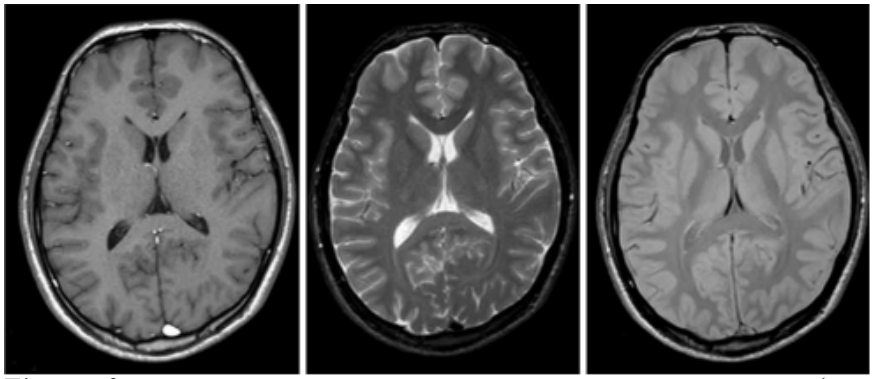

Figure 8. In vivo brain T_1, T_2 and PD weighted images (left to right). Each images show different contrasts which gives useful information about the composition and characteristics of tissues in clinical application.

1.5 Quantitative MRI

Recent advancement of MR hardware, signal processing method and novel understanding of biophysics lead to the revitalization of the imaging method called *quantitative MR imaging* (qMRI). qMRI has important meaning in terms of quantifying the tissue characteristics enabling earlier and more rigorous diagnosis of diseases and also quantitative analysis in scientific applications. There are many qMRI imaging methods available, but here we introduce some methods which are relevant to this study: R_2 and R_2' mapping and Quantitative Susceptibility Mapping (QSM).

1.5.1 R_2 and R_2' mapping

R_2 is inverse of T_2 ($R_2 = 1/T_2$) and it is usually measured by multiple acquisitions of single-echo spin echo sequence or multi-echo spin echo pulse sequence [3,4]. R_2 decay is derived from the natural interactions of spins at atomic and molecular levels such as dipolar interaction and contributes the decay of transverse magnetization.

R_2^* ($R_2^* = 1/T_2^*$) decay is originated from multiple sources that lead to field inhomogeneities such as air cavities (e.g. sinus) and susceptibility sources (e.g. ferritin cluster, contrast agents). To measure R_2^*, multi-echo *gradient echo* (GRE) pulse sequence is acquired. This pulse sequence does not include the refocusing pulse compared to spin echo pulse sequence and only compose of acquisition of multiple echoes after excitation pulse. Then, R_2' can be defined as follows:

$$1/T_2' = 1/T_2^* - 1/T_2 \qquad \text{[Eq. 3]}$$

or equivalently,

$$R_2' = R_2^* - R_2 \qquad \text{[Eq. 4]}$$

R_2' is a reversible signal component which reflects the field inhomogeneity effects [5] **(Fig. 9)**.

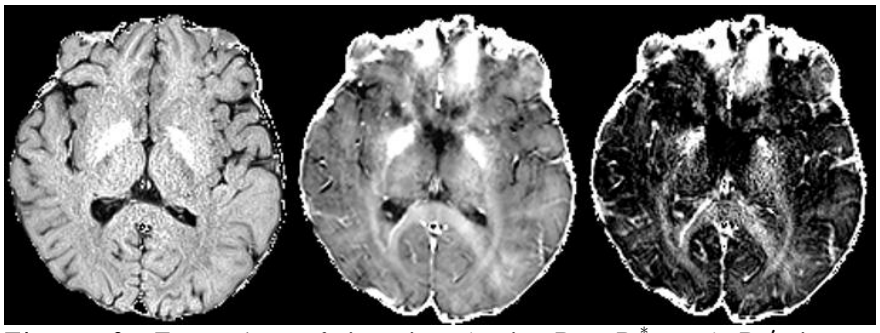

Figure 9. Examples of in-vivo brain R_2, R_2^* and R_2' image contrasts (left to right). R_2^* image shows severe distortion and hyper-intensity in the frontal lobe due to macroscopic field inhomogeneity. In contrast, R_2 image shows clear description of anatomical regions in frontal lobe by compensating spin dephasing because of the phase reversal induced by the refocusing pulse.

1.5.2 Quantitative Susceptibility Mapping (QSM)

Quantitative Susceptibility Mapping (QSM) is a novel contrast mechanism that its intensity is linearly proportional to the magnetic susceptibility of tissue within a voxel. In acquisition, 3D multi-echo GRE pulse sequence is usually used with high resolution.

The processing pipeline of QSM is shown in **Figure 10**. First, GRE phase data is scaled by the TE and gyromagnetic ratio to acquire the local frequency shift. After local frequency shift is isolated, this data have to be further processed to remove phase wrapping and background field perturbations. Phase unwrapping can be performed using several algorithms including Laplacian based approach [6].

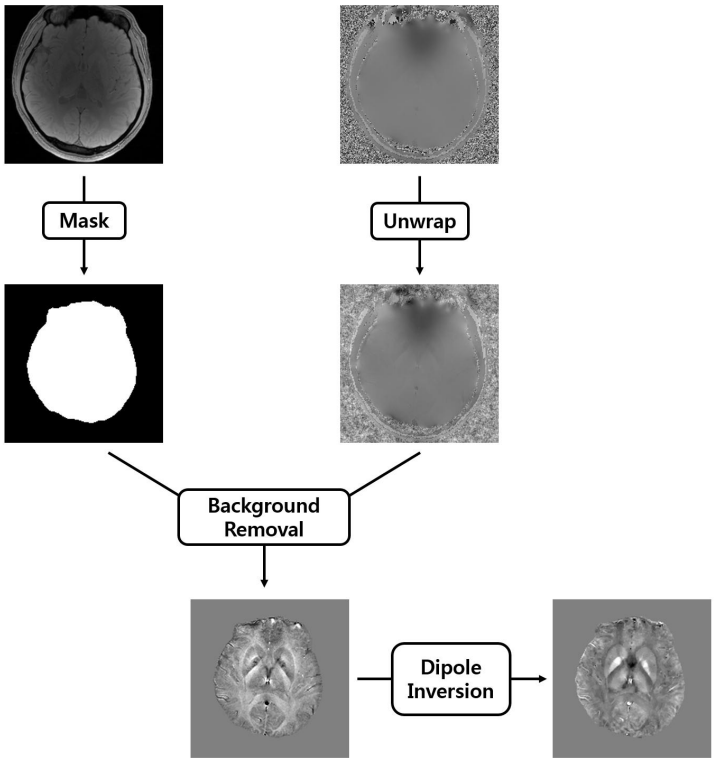

Figure 10. Processing pipeline of QSM reconstruction. GRE phase and magnitude data is processed in several steps to extract magnetic susceptibility insdie a voxel from a local frequency shift.

Background field removal also can be done using a number of algorithms including PDF [7], SHARP [8], HARPERELLA [9]. In the process of background field removal, GRE magnitude image is used to mask volume of interest (VOI) to separate brain and background. If we acquire a local tissue field map using phase unwrapping and background field removal algorithms successfully, we are now ready to recover a susceptibility map by deconvolving the field map with the unit dipole kernel. Actually, the deconvolution is

exactly same as a pointwise division in k-space shown in the following formula:

$$\Delta B_z(k) = B_0\left(\frac{1}{3} - \frac{k_z^2}{|k^2|}\right)\chi(k) \qquad \text{[Eq. 5]}$$

where k is k-space vector and B_0 is applied static magnetic field. $\Delta B_z(k)$ and $\chi(k)$ are the Fourier transform of a local field map and susceptibility map. However, this deconvolution is ill-posed problem because dipole kernel in k-space includes many zeros in the two conical surfaces at approximately 54.7° with respect to the main magnetic field. Several strategies have been proposed including MEDI method [10] which is based on L1-norm regularization to reduce or eliminate artifacts coming from missing data in zero cone.

2. Proposed Methods

2.1 Introduction

Quantitative MR imaging (qMRI) is an important method in exploring tissue composition and properties [11,12]. qMRI, however, is hindered by a long acquisition time in obtaining multiple contrast images. In this work, we demonstrated that a modified gradient-echo sampling of FID and echo (mGESFIDE) sequence [13,14] could obtain multiple contrast images (R_2, R_2', R_2^*, local field map, QSM, positive and negative susceptibility maps [15]) in 5 minutes of scan time. In particular, we developed a new algorithm for improved R_2 and R_2' maps by considering RF slice profiles in the excitation and refocusing RF pulses and B_1 inhomogeneity. Additionally, we developed a method that generated a high quality local field map by utilizing all echoes of mGESFIDE.

2.2 Methods

2.2.1 mGESFIDE pulse sequence

Ma. et al at 1995 [13] proposed the new data acquisition strategy called GESFIDE which samples whole signal trajectory before and after the refocusing pulse in spin echo sequence. This method has several advantages compared to traditional SE and GRE experiments and one of those advantages is the ability to measure the irreversible and

reversible relaxation rate (R_2 and R_2') in a single scan. mGESFIDE pulse sequence is a modified version of GESFIDE sampling strategy. It keeps sampling the echoes after refocusing echo time while GESFIDE samples the echoes until the refocusing echo time only. mGESFIDE pulse sequence diagram is shown in **Figure 11**. In this figure, total 20 echoes are acquired with 7 echoes before the refocusing pulse and 13 echoes after the refocusing pulse. In this study, we introduce the signal model which describes mGESFIDE signal trajectory in mathematical form.

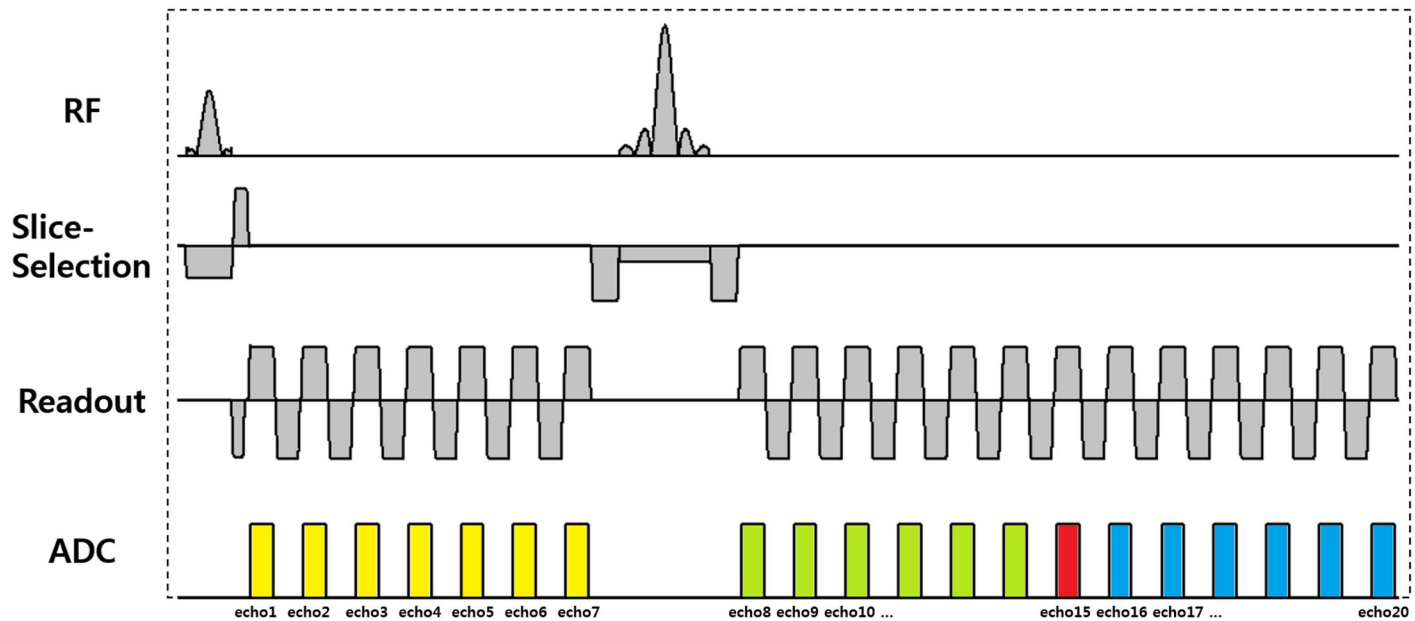

Figure 11. Pulse sequence diagram for mGESFIDE. 20 echoes were acquired in total (7 echoes before the refocusing pulse and 13 ecehos after the refocusing pulse).

2.2.2 Improved R_2 and R_2' estimation

Overall data processing pipeline is summarized in **Figure 12**. A novel R_2 and R_2' estimation method incorporated the excitation and refocusing slice profiles and also B_1 inhomogeneity factor in the signal model which is expressed as follows:

$$S(TE)=\begin{cases}\sum_z \sin(B_1\,\alpha(z))\exp(-(R_2+R_2')\,TE) & TE<\frac{TE_{ref}}{2}\\ \sum_z \sin(B_1\,\alpha(z))\frac{1-\cos(B_1\,\beta(z))}{2}\exp(-R_2\,TE)\exp(-R_2'|TE-TE_{ref}|) & TE>\frac{TE_{ref}}{2}\end{cases}$$

[Eq. 6]

where α and β are excitation and refocusing flip angles calculated by RF slice profiles sampled with 200 points along the z-direction denoted by z [16], S is a generated signal, B_1 is B_1 inhomogeneity scaling factor, TE is echo time and TE_{ref} is refocusing echo time. To estimate R_2 and R_2', nonlinear optimization method (lsqnonlin in MATLAB; tolerance = 1e-6) was applied with initial values (R_2 = 10 Hz, R_2' = 5 Hz, B_1 = 1). The results of this method were compared with those from the conventional GESFIDE processing which does not incorporate slice profiles information and B_1 inhomogeneities. The additional comparison was performed with the results from GRE and SE sequences.

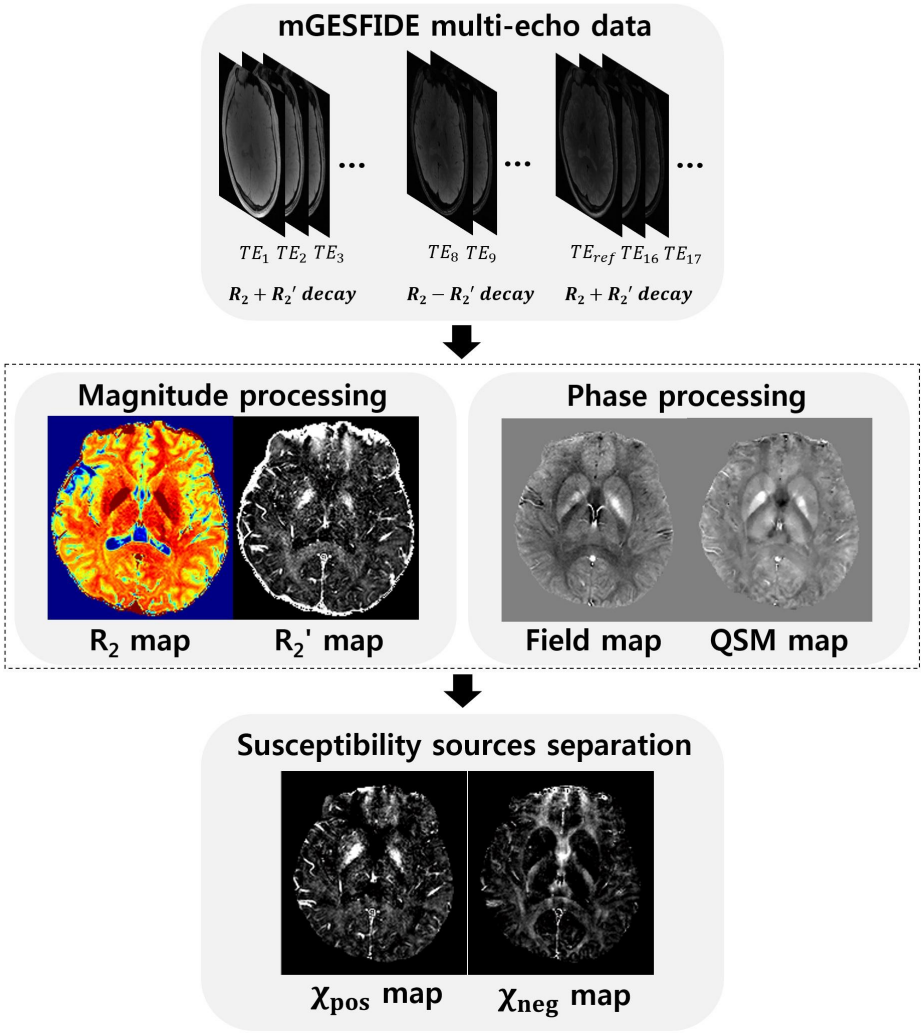

Figure 12. mGESFIDE data processing pipeline. R_2 and R_2' values are obtained by fitting the magnitude data to the signal model in **Eq. 6**. The local field map is generated by solving **Eq. 7** and QSM map is reconstructed using MEDI. Susceptibility sources separation is achieved using R_2' and local field estimation.

2.2.3 Novel local field map estimation

For a reliable estimation of the field map in mGESFIDE pulse sequence, a new method utilizing all echoes of mGESFIDE signal was developed. The method was performed by solving the minimization problem given as follows:

$$\begin{aligned}\mathrm{argmin}_{f,\Phi_0,\Phi_1} &\sum_{TE_j < TE_{ref}/2} \|S(TE_j) - A(TE_j)\exp(i(f\,TE_j + \Phi_0))\|_2^2 \\ &+ \sum_{TE_j > TE_{ref}/2} \|S(TE_j) - A(TE_j)\exp(i(f\,TE_j + \Phi_1))\|_2^2\end{aligned}$$

[Eq. 7]

where f represents the frequency shift of a voxel which is same before and after the refocusing RF pulse, Φ_0 and Φ_1 are different phase offsets before and after the refocusing RF pulse, S is complex data, A is signal magnitude. The cost function was linearized and updated iteratively [17]. From f, local field was estimated [7]. For comparison, complex multi-echo GRE data were also processed for a local field map. QSM maps were generated from the local field maps using MEDI [10].

2.2.4 Susceptibility source separation

Since our sequence provides both R_2' and local field maps, one can perform susceptibility sources separation to generate positive and negative susceptibility source maps (χ_{pos} and χ_{neg}) as suggested in [15]. The results were

compared with the maps generated using R_2' and local field maps from the SE and GRE.

2.2.5 In vivo study

Data was collected at 3T using 2D mGESFIDE sequence. Total 20 echoes were acquired before (3:3:21 ms, 7 echoes) and after the refocusing RF pulse (31:3:67 ms, 13 echoes). The scan parameters were as follows: TR = 3000 ms, voxel size = 1x1 mm^2, number of slice = 40 and scan time = 5:36 minutes. For comparison, 2D multi-echo SE and GRE were acquired (SE: 7 echoes with 10:10:70 ms, TR = 3500 ms; GRE: 7 echoes with 3.06:4.59:30.6 ms, TR = 2400 ms; other parameters were the same). The total scan time for SE and GRE was 14:55 minutes.

First, R_2 and R_2' maps from the proposed method were compared with the maps from the conventional GESFIDE method to show the superiority of this new fitting method **(Eq. 6)**. Next, several image contrasts reconstructed from the mGESFIDE acquisition were compared with the ones from the SE and GRE acquisitions to validate agreement between two methods.

2.3 Results

Figure 13 compares R_2 and R_2' maps from conventional GESFIDE processing [13] and the proposed method. At a glance, the maps from the proposed method shows higher

image quality than the conventional maps. Especially, R_2 map shows relatively high SNR compared to conventional one and also R_2' map shows higher image contrasts compared to the one from conventional GESFIDE.

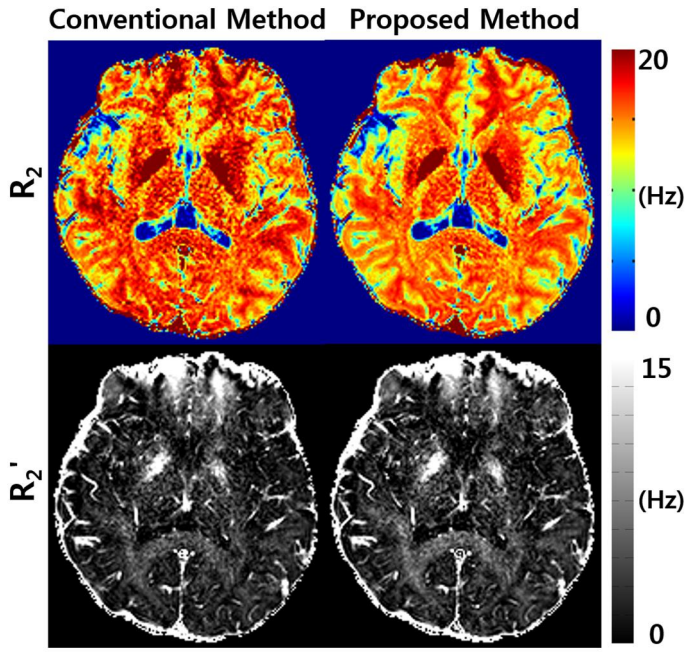

Figure 13. Comparison of R_2 and R_2' maps from conventional GESFIDE processing and the proposed method. The R_2 and R_2' maps from the proposed method show higher SNR than those from the conventional method. The consideration of the slice profiles and B_1 inhomogeneities in the new processing may explain the improvement.

Figure 14 summarizes the R_2, R_2', R_2^*, QSM, χ_{pos} and χ_{neg} maps for a representative slice from the conventional

approaches (left column: GRE and SE results) and the new reconstruction approaches (right column: mGESFIDE results). The QSM results show a high similarity between the two methods. Both χ_{pos} and χ_{neg} maps also show similar contrasts. For example, deep grey matter such as globus pallidus has high intensity in both χ_{pos} maps whereas χ_{neg} maps show unnoticeable signal in these regions. The R_2 map from the proposed methods shows higher values globally than the one from SE, which may be explained by diffusion effect [18,19].

For further investigation, we also compared mean ROI values in 5 ROIs including PU(putamen), GP(globus pllidus), TH(thalamus), SP(splenium), OP(optic radiation). Each ROIs is manually segmented. As shown in **figure 15 and 16**, Large deviation of R_2 and R_2^* values are observed in deep grey matter (PU, GP) compared to relatively small deviation of values in white matter fiber (SP, OP). In this deep grey regions, diffusion effect would be significant due to large amount of susceptibility sources.

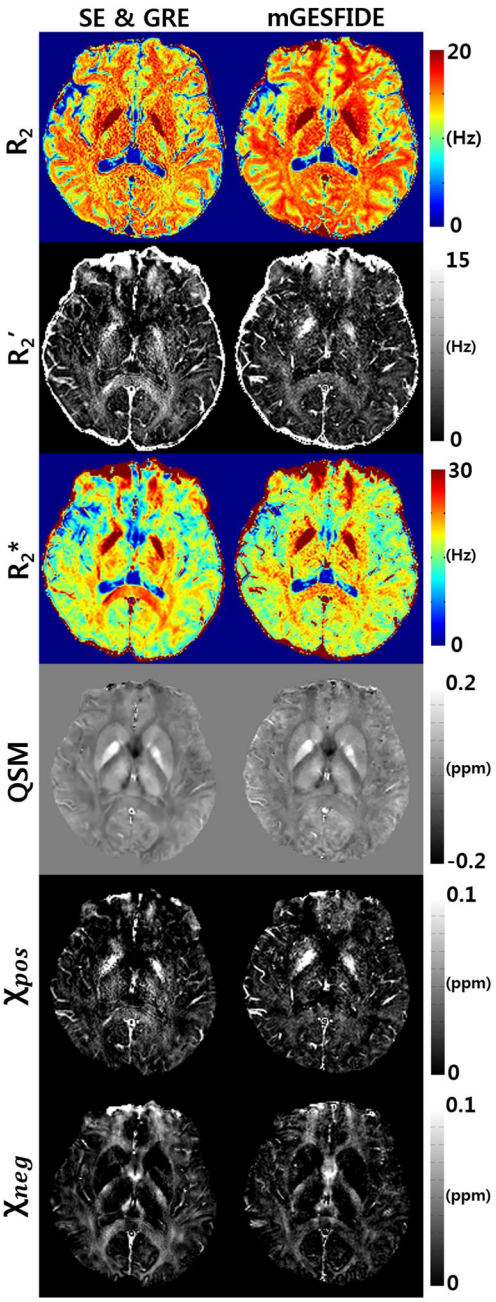

Figure 14. Comparison of the six image contrasts from the conventional and the new approaches.

Proposed method (mGESFIDE)

	PU	GP	TH	SP	OP
R2	16.59(1.55)	26.19(2.49)	16.10(1.52)	15.37(1.20)	14.93(0.92)
R2*	20.20(3.30)	40.02(7.02)	19.40(2.91)	21.64(2.15)	19.61(2.41)
R2'	3.60(3.12)	13.8(5.89)	3.29(2.49)	6.27(1.79)	4.67(2.21)

Conventional method (SE & GRE)

	PU	GP	TH	SP	OP
R2	15.76(1.94)	22.55(4.26)	15.60(2.48)	14.68(3.28)	13.68(1.53)
R2*	17.56(4.09)	32.50(7.16)	19.69(2.57)	22.53(2.84)	20.13(1.80)
R2'	1.80(4.33)	9.94(5.82)	4.08(3.40)	7.84(3.07)	6.45(2.42)

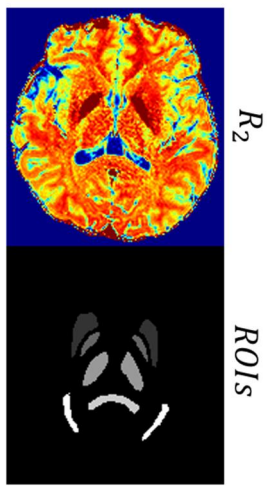

Figure 15. Mean and standard deviation of ROIs in R_2, R_2' and R_2^* maps. R_2 map and ROI map is shown on the right side for convenience.

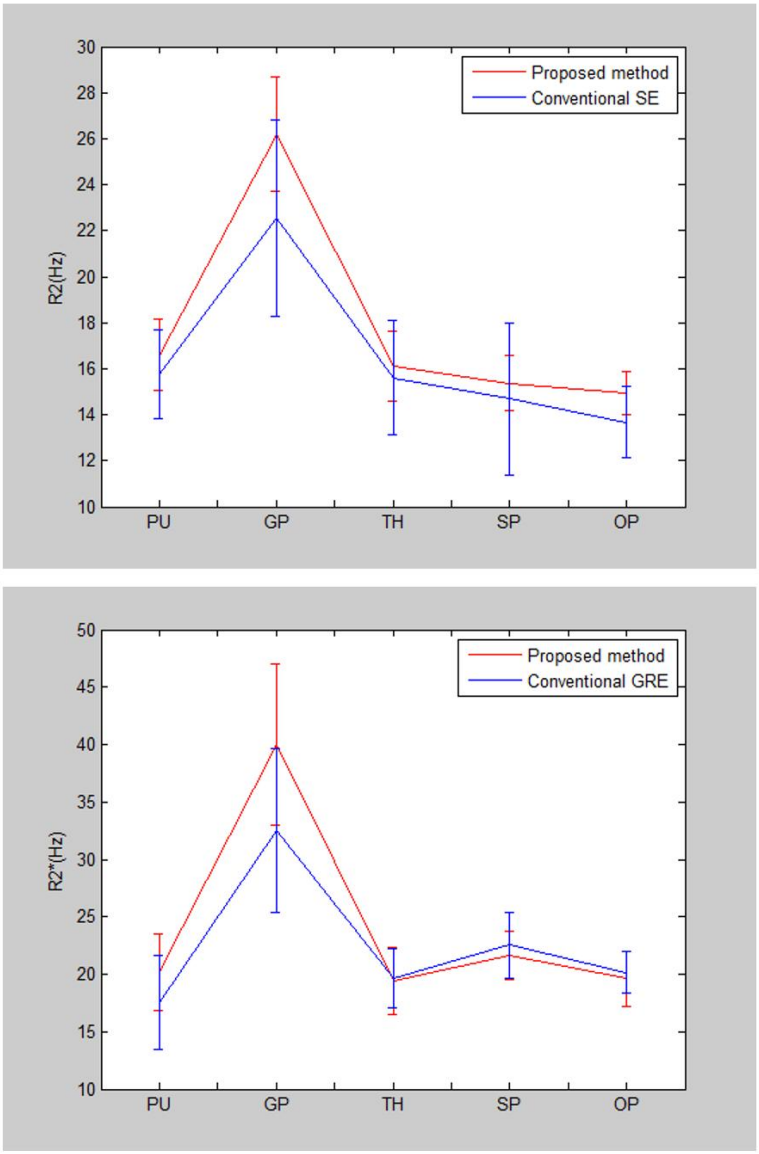

Figure 16. Line plot of mean values of each ROIs. Large deviation between two methods are observed in deep grey matter including PU and GP because diffusion effect would be significant due to large amount of susceptilibty sources.

3. Discussion and Conclusions

Quantitative MR imaging (qMRI) has important role in the growing of the need for quantitative analysis in MR imaging. However, most of pulse sequences for qMRI takes long time to extract quantitative information of tissue.

In this work, we demonstrated that mGESFIDE pulse sequence produces six images contrasts in just 5 minutes of scan time. We introduced the novel techniques which improved the quality of R_2 and R_2' maps, suggesting that the slice profiles and B_1 inhomogeneity factor need to be included in the model. Additionally, we proposed the new fitting method for field map estimation which utilized whole echoes of mGESFIDE pulse sequence.

We validated our method by comparing the conventional approaches to the proposed method. All six quantitative images have very similar contrasts globally although R_2 has higher values in the proposed method which may be originated from the diffusion effect contributing the signal reduction after the refocusing pulse.

New method using mGESFIDE acquisition has potential to map the quantitative multi-modal information rapidly and this advantage lead to application of quantitative analysis in neuroscience and more advanced clinical diagnosis using several quantitative information of tissues.

4. References

[1] 김재형. "T1, T2 강조영상, FLAIR 영상의 임상 적용." 대한자기공명의과학회지 13 (2009): 9-14.

[2] Damadian, Raymond. "Tumor detection by nuclear magnetic resonance." (1971): 1151-1153.

[3] Hahn, Erwin L. "Spin echoes." Physical review 80.4 (1950): 580.

[4] Carr, Herman Y., and Edward M. Purcell. "Effects of diffusion on free precession in nuclear magnetic resonance experiments." Physical review 94.3 (1954): 630.

[5] Yablonskiy, Dmitriy A., and E. Mark Haacke. "Theory of NMR signal behavior in magnetically inhomogeneous tissues: the static dephasing regime." Magnetic resonance in medicine 32.6 (1994): 749-763.

[6] Jenkinson, Mark. "Fast, automated, N-dimensional phase-unwrapping algorithm." Magnetic resonance in medicine 49.1 (2003): 193-197.

[7] Liu, Tian, et al. "A novel background field removal method for MRI using projection onto dipole fields." NMR in Biomedicine 24.9 (2011): 1129-1136.

[8] Schweser, et al. "Quantitative imaging of intrinsic magnetic tissue properties using MRI signal phase: an approach to in vivo brain iron metabolism?." Neuroimage 54.4 (2011): 2789-2807.

[9] Li, Wei, et al. "Integrated Laplacian-based phase unwrapping and background phase removal for quantitative susceptibility mapping." NMR in Biomedicine 27.2 (2014): 219-227.

[10] Liu, Jing, et al. "Morphology enabled dipole inversion for quantitative susceptibility mapping using structural consistency between the magnitude image and the susceptibility map." Neuroimage 59.3 (2012): 2560-2568.

[11] Lorio, Sara, et al. "Neurobiological origin of spurious brain morphological changes: a quantitative MRI study." Human brain mapping 37.5 (2016): 1801-1815.

[12] Petiet, Alexandra, Marie-Stephane Aigrot, and Bruno Stankoff. "Gray and White Matter Demyelination and Remyelination Detected with Multimodal Quantitative MRI Analysis at 11.7 T in a Chronic Mouse Model of Multiple Sclerosis." Frontiers in neuroscience 10 (2016).

[13] Ma, Jingfei, and Felix W. Wehrli. "Method for image-based measurement of the reversible and irreversible contribution to the transverse-relaxation rate." Journal of Magnetic Resonance, Series B 111.1 (1996): 61-69.

[14] Ni, Wendy, et al. "Comparison of R2′ measurement methods in the normal brain at 3 Tesla." Magnetic resonance in medicine 73.3 (2015): 1228-1236.

[15] Lee et al. Separating postivie and negative susceptibility sources in QSM. ISMRM. 2017.

[16] Pauly, John, et al. "Parameter relations for the Shinnar-Le Roux selective excitation pulse design algorithm (NMR imaging)." IEEE transactions on medical imaging 10.1 (1991): 53-65.

[17] Liu, Tian, et al. "Nonlinear formulation of the magnetic field to source relationship for robust quantitative susceptibility mapping." Magnetic resonance in medicine 69.2 (2013): 467-476.

[18] Jensen, J. H., R. Chandra, and Hao Yu. "Quantitative model for the interecho time dependence of the CPMG relaxation rate in iron-rich gray matter." Magnetic resonance in medicine 46.1 (2001): 159-165.

[19] Stefanovic, Bojana, John G. Sled, and G. Bruce Pike. "Quantitative T2 in the occipital lobe: the role of the CPMG refocusing rate." Journal of Magnetic Resonance Imaging 18.3 (2003): 302-309.